Study of the Lifetime of High-Power GaAs PCSSs Under Different Energy Storage Modes

Cheng Ma, Lei Yang, Shaoqiang Wang, Yu Ji, Lin Zhang, and Wei Shi

***Abstract*—This paper presents an experimental study on the lifetime of high-power gallium arsenide photoconductive semiconductor switches (PCSSs) under different energy storage modes. Under the capacitive energy storage mode, the lifetime of a PCSS was increased by a factor of 10 through a reduction in the capacitor size, which reduces the hold-time of the carrier avalanche multiplication. Under the transmission line energy storage mode, the lifetime of a PCSS was increased by more than twofold by reducing the bias electric field, which reduces the degree of the carrier avalanche multiplication. Additionally, the influence of various factors on device lifetime and the failure mechanisms are discussed. The experimental results and analysis indicate that electrode erosion and stress damage are the two leading factors that induce the failure of high-power PCSSs.**

***Index Terms*—Power semiconductor switches, semiconductor device breakdown, semiconductor device reliability, semiconductor device thermal factors, semiconductor switches.**

I. Introduction

PHOTOCONDUCTIVE semiconductor switches (PCSSs) are optically triggered switches that offer improvements for existing and future pulsed power systems. They are currently being tested for use in high-impedance, low-current applications, as well as in high-voltage, high-current applications [1]–[5]. For example, munitions firing sets require a PCSS that can operate at 1 kV and 1 kA with a compact package, and electrooptic drivers require a PCSS that can switch a current of 100 A at 3–6 kV with a rise time on the order of hundreds of picoseconds. PCSS arrays are also used to generate high-power ultrawideband microwave radiation due to their fast rise time, and this application requires all PCSSs elements to be synchronized with each other. High-power PCSSs exhibit a number of advantages when compared to conventional switches, including high-speed response to laser pulses, higher power capabilities, optical electrical isolation, and a low laser energy trigger requirement.

Manuscript received February 5, 2016; revised May 22, 2016; accepted August 11, 2016. Date of publication August 16, 2016; date of current version February 11, 2017. This work was supported in part by the National Basic Research Program of China ("973" Program) under Grant 2014CB339800, in part by the National Natural Science Foundation of China under Grant 61427814 and Grant 51377133, in part by the Ultrafast Photo-Electronic Technology Innovation Group of Shaanxi Province under Grant 2014KCT-13, and in part by the Terahertz Science and Technology Fund of the Chinese Academy of Engineering Physics under Grant CAEPTHZ201404. Recommended for publication by Associate Editor K. Sheng. *(Corresponding author: Wei Shi.)*

The authors are with the Research Center for Ultrafast Photoelectric Technology, Xi'an University of Technology, Xi'an 710048, China e-mail: swshi@mail.xaut.edu.cn).

Color versions of one or more of the figures in this paper are available online at http://ieeexplore.ieee.org.

Digital Object Identifier 10.1109/TPEL.2016.2600959

A PCSS has two operating modes: linear mode and nonlinear mode. In the linear mode, each photon that is absorbed induces the formation of one electron–hole pair. Consequently, the output current waveform is similar to laser pulse waveform. In this case, the rise time of the current is determined primarily by the rise time of optical trigger. The nonlinear mode is also known as "lock-on" or "high-gain," and it relies on the process of multiplication of the photon-induced carriers in the bulk of the GaAs material [6]. In this mode, a single incident photon will ultimately induce the formation of multiple electron–hole pairs. In general, the PCSS remains locked in the "ON" state even after the laser trigger is removed, provided that the external circuit can supply the required power. In this mode, the current path through the device is filamentary channel [7].

The lock-on behavior of a PCSS in the nonlinear mode of operation has been widely used in high-voltage and high-power applications [8]–[11]. However, the high currents through the filaments in this mode have a serious influence on the lifetime of devices [12], [13]. The damage to the surface of high-power PCSSs reduces their lifetime, which makes these devices unsuitable for use in many important application areas. This paper focuses on improving PCSS lifetime through improvements in the switch contacts, energy storage mode, and the charging mechanism. This paper has presented that the PCSS lifetime is improved by decreasing capacitance to control the hold-time of carrier avalanche multiplication and changing bias electric field to control the avalanche degree.

The organization of this paper is as follows. The structure of the PCSS and the experimental setups to evaluate its performance will be described in Section II. Section III will present and discuss the experimental results, and conclusions will be presented in Section IV.

II. Experimental Setup

In our experiments, the photoconductive material used for the PCSSs is semiinsulating (SI) GaAs. SI-GaAs is a direct bandgap semiconductor with a bandgap energy of 1.42 eV. The dark (nonilluminated) resistivity of SI-GaAs is greater than $5 \times 10^7\ \Omega$·cm, and the electron mobility is higher than 5000 $cm^2/(V{\cdot}s)$. The overall size of the SI-GaAs substrate is 10.0 mm (width) × 15.0 mm (length) × 0.6 mm (thickness). The PCSS has a lateral (or horizontal) structure, as shown in Fig. 1.

Ohmic contact electrodes are placed on both sides of the substrate surface, and are composed of an Au/Ge/Ni alloy. The size of each electrode is 6.0 mm × 3.0 mm, and they feature two optimizations to improve the PCSS lifetime: the corners

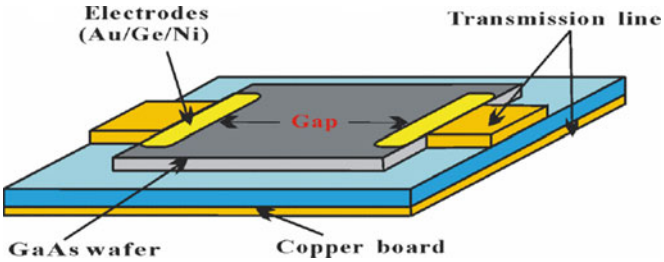

Fig. 1. Schematic diagram of a high-power GaAs PCSS.

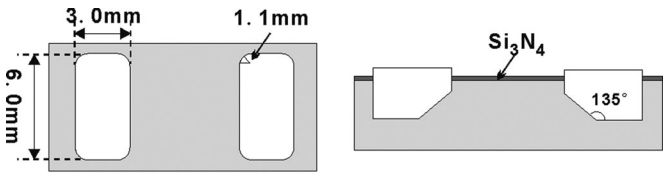

Fig. 2. Schematic diagram of the SI-GaAs PCSS electrodes. (a) Top view of electrodes. (b) Side profile of electrodes.

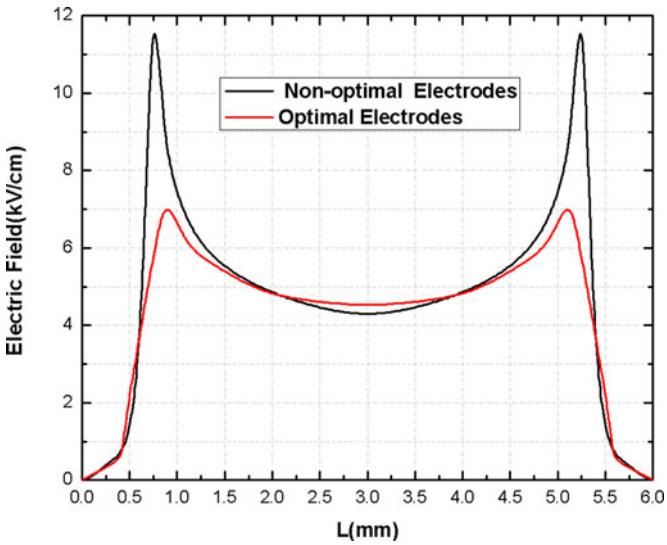

Fig. 3. Electric field distribution curves for optimal electrodes and nonoptimal electrodes.

are rounded with a 1.1 mm radius [as shown in Fig. 2(a)], and an optimal etch angle of 135° was used [as shown in Fig. 2(b)]. These optimizations reduce the electric field strength at the electrode edges and improve PCSS lifetime, as shown in Fig. 3. A 900-nm Si_3N_4 film is used to coat the surface of the GaAs PCSS for insulating protection. The switch is placed on a Teflon substrate with planar transmission lines, and it connects with the external circuit through coaxial transmission lines.

The performance of this device will be evaluated in experiments that use both capacitive and transmission line energy storage, as described in the following sections.

A. Capacitive Energy Storage Mode

In this experiment, a ceramic capacitor is charged by a high-voltage dc power supply through a 10-MΩ resistor and then discharged through a PCSS. The PCSS is triggered by a laser

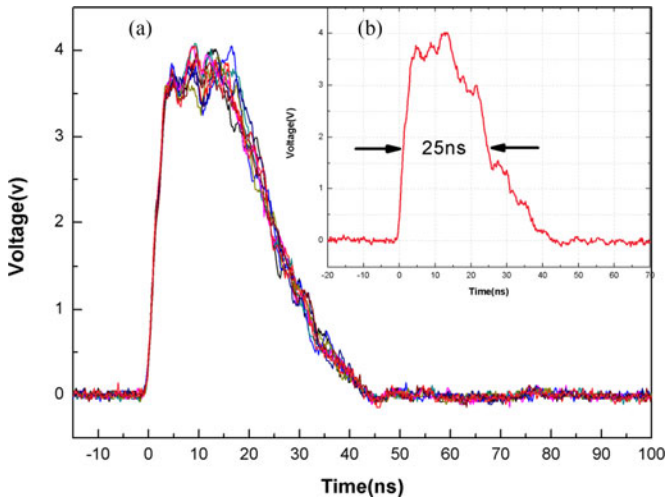

Fig. 4. LD pulse waveform. (a) Superposition of ten waveforms. (b) Single waveform.

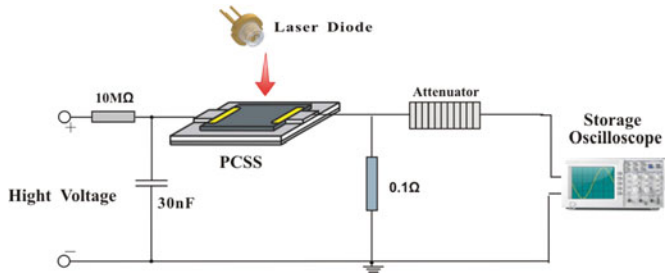

Fig. 5. Test circuit for a 3-mm-gap GaAs PCSS with a 30-nF energy storage capacitor.

diode (LD), which emits a 25 ns pulse with an energy of 1.6 μJ and a wavelength of 905 nm. The laser pulse was the entire gap illuminated. Fig. 4 shows the superposition of ten emitted laser pulse waveforms, along with the waveform of a single pulse for clarity.

In the first test, a PCSS with a 3-mm gap is charged by a 30-nF capacitor as shown in Fig. 5. Once the switch is triggered, the capacitor is discharged through the switch and a 0.1-Ω current-viewing resistor (CVR). The voltage across the CVR is attenuated by a 60-dB coaxial attenuator and measured by a digital storage oscilloscope (LeCroy WaveRunner 64Xi) with a 600 MHz bandwidth. The current through the CVR can be calculated from the measured voltage.

In the second test, a PCSS with a 2-mm gap is charged by a 470-nF capacitor as shown in Fig. 6. Once the switch is triggered, the capacitor is discharged through the switch and a 0.1-Ω load resistor. The current through the PCSS and resistor is measured using a current monitor (Pearson Model 7427) with a 70 MHz bandwidth, and this is recorded by the same digital storage oscilloscope used in the first test.

B. Transmission Line Energy Storage Mode

This experiment consists of a high-power pulsed system with a parallel-plate Blumlein line (BL) structure. A plate transmission line is formed by using a ceramic dielectric with silver electrodes printed on both sides. The size of the ceramic

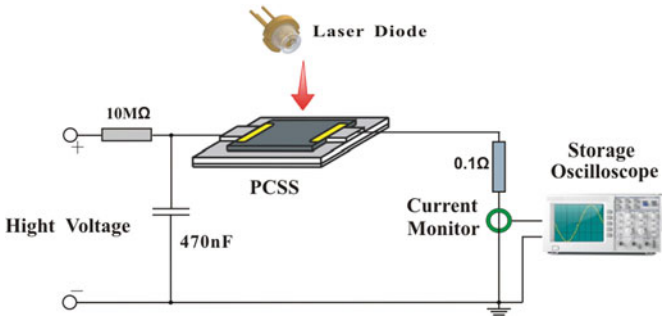

Fig. 6. Test circuit for a 2-mm-gap GaAs PCSS with a 470-nF energy storage capacitor.

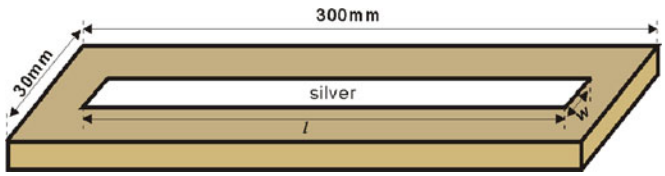

Fig. 7. Structure of the plate transmission line.

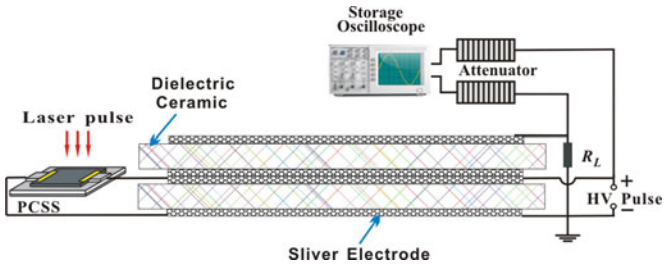

Fig. 8. Transmission line energy storage test circuit for the GaAs PCSS.

dielectric is 300.0 mm × 30.0 mm, and each silver electrode is 280.0 mm × 4.0 mm. The structure of the plate transmission line is shown in Fig. 7, and a BL is formed by stacking two plate transmission lines.

The test circuit for the GaAs PCSS is shown in Fig. 8. The BL is charged by a high-voltage pulse, and a SI-GaAs PCSS and a 150 Ω load are attached to the beginning and end of the BL, respectively. The SI-GaAs PCSS is triggered by a Nd:YAG solid-state laser, which emits a 9.5 ns pulse with an energy of 76 mJ and a wavelength of 1064 nm. The laser pulse was the entire gap illuminated. Fig. 9 shows the superposition of ten emitted laser pulse waveforms, along with the waveform of a single pulse for clarity. The input bias voltage on the GaAs PCSS and the output voltage across the load are attenuated by 60-dB coaxial attenuators and measured by a digital storage oscilloscope (LeCroy HDO4104) with a 1 GHz bandwidth.

III. Results and Discussion

A. Capacitive Energy Storage Mode

Using the capacitive energy storage mode experimental setups described in the previous section, we can analyze the discharge properties of the switch and gain insight into how the GaAs PCSS exits from the nonlinear mode of operation and turns

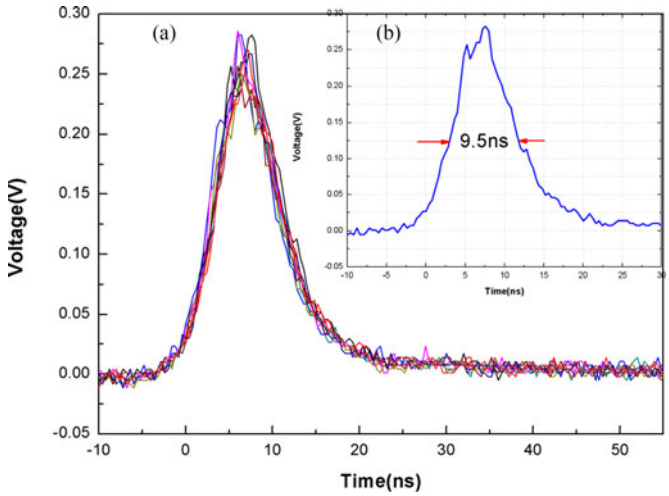

Fig. 9. Nd:YAG solid-state laser pulse waveform. (a) Superposition of ten waveforms. (b) Single waveform.

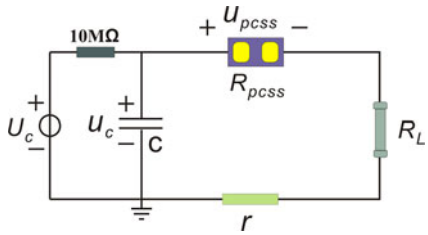

Fig. 10. Lumped-parameter circuit model of the experiment circuit.

off. This requires an understanding of the transient current and electric field characteristics of the PCSS. The lumped-parameter circuit model of the circuit used in these experiments is shown in Fig. 10 [14].

The transient characteristics of the PCSS can be expressed as follows:

$$E(t) = \frac{Q_C(t)/C - I(t)\cdot(R_L + r)}{L_{\text{gap}}} \tag{1}$$

where E is the average electric field of the PCSS, Q_C is the charge stored in the capacitor, R_L is the load resistance, r is the parasitic resistance (∼1 Ω), and L_{gap} is the gap of PCSS. The discrete-time data of for the current I are obtained from the oscilloscope.

Fig. 11 shows the current and the electric field characteristic curves for a 2-mm-gap GaAs PCSS. The bias voltage is 1950 V, and the ceramic capacitor has a value of 470 nF. When the biasing electric field is higher than the nonlinear threshold electric field (as determined primarily by the characteristics of the PCSS), the PCSS operates in the nonlinear mode. In this particular test, the nonlinear threshold electric field is taken as 8.2 kV/cm [15]. When the LD triggers the PCSS, a number of photon-activate carriers form a photon-activated charge domain (PACD) in the PCSS. Meanwhile, a high local electric field in the PACD satisfies the avalanche breakdown condition. Avalanche impact ionization causes carrier avalanche multiplication, which results in a rapid increase in the current.

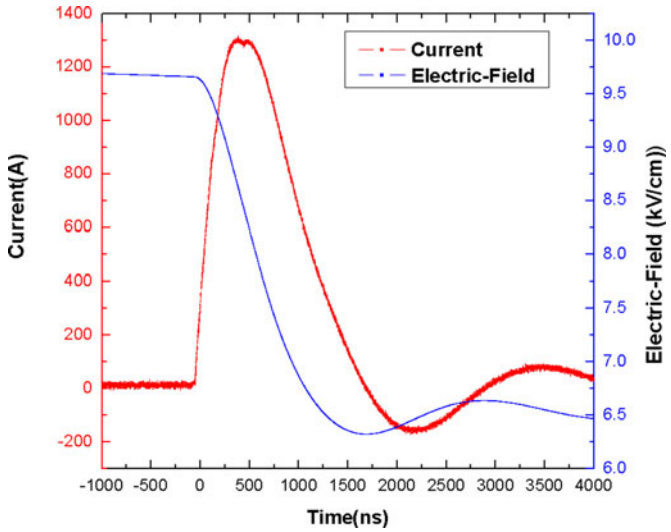

Fig. 11. Current and electric field characteristic curves for a 2-mm-gap GaAs PCSS.

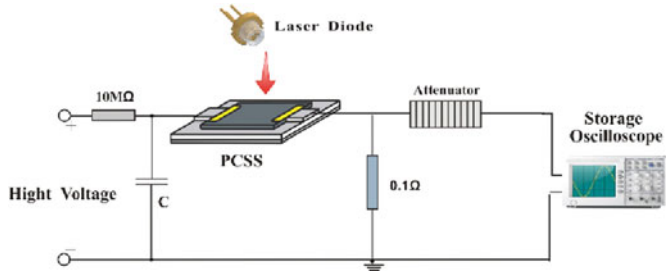

Fig. 12. Test circuit for a 3-mm-gap GaAs PCSS with different energy storage capacitors.

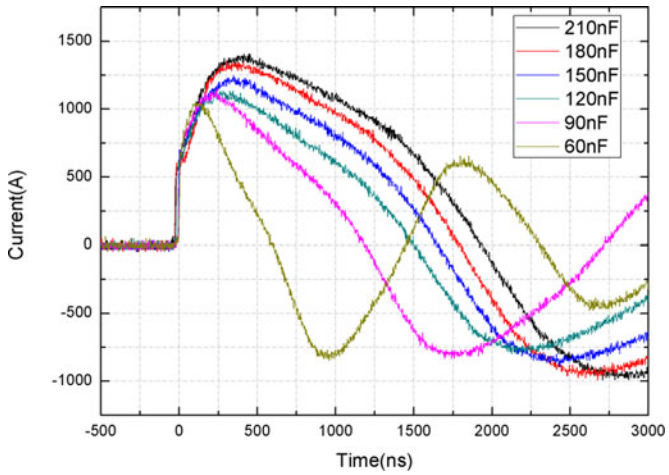

Fig. 13. Current waveforms of 3-mm-gap PCSSs charged by different capacitors at 4 kV bias voltage.

TABLE I
SUMMARY OF THE CAPACITIVE TEST PARAMETERS AND RESULTS

THE VALUE OF CAPACITOR	Pulse width	Lifetime
210 nF	1500 ns	One shot
180 nF	1400 ns	One shot
150 nF	1250 ns	Two shots
120 nF	1100 ns	Two shots
90 nF	750 ns	Five shots
60 nF	400 ns	Seven shots

The blue line in Fig. 11 shows that the electric field in the PCSS rapidly decreases toward the nonlinear threshold electric field (∼8 kV/cm) as soon as the discharge process begins. Once the electric field across the PCSS reaches the threshold electric field, the carrier recombination rate is equal to the production rate. After a few nanoseconds, the circuit discharge causes the electric field across the switch to drop below the level required to sustain the PACD. The current begins to drop significantly as soon as the PCSS exits the nonlinear mode of operation because the carrier avalanche multiplication process stops.

The previous analysis indicates that the hold-time of the carrier avalanche multiplication is dominated by the value of the capacitance. When the PCSS operates in an avalanche multiplication mode, the current path in the device is through filaments. This high level of current can cause thermal breakdown in the filaments, which has a serious influence on the lifetime of the PCSS. In order to improve the lifetime of PCSS, the capacitor of the test circuit is changed to reduce the hold-time of the carrier avalanche multiplication. In the new test, a PCSS with a 3-mm gap is charged by some different energy storage capacitors (210, 180, 150, 120, 90, 60 nF) as shown in Fig. 12. Fig. 13 shows current waveforms of 3-mm-gap PCSSs charged by different capacitors at 4 kV bias voltage. It is clearly observed that pulse width of current waveform decreases with the decrease of the value of a ceramic capacitor. The test results indicate that the hold-time of the carrier avalanche multiplication is dominated by the value of the capacitance.

The PCSS lifetime and capacitance parameters for these tests are summarized in Table I. This table shows that the PCSS lifetime increases with decreasing capacitance. And it is clearly observed that the peak value of the current decreases with decreasing capacitance. To maintain consistency of the peak value of the current under the different capacitances, it is required to increase bias electric field. So, we have increased bias electric field through changing the bias voltage and the gap of GaAs PCSS.

Fig. 14 shows the current and the electric field characteristic curves for a 3-mm-gap GaAs PCSS. The bias voltage is 4800 V, and the ceramic capacitor has a value of 30 nF. In this case, a breakdown occurred after ten pulses. The blue line in Fig. 14 shows that the electric field of the PCSS decreases rapidly to the nonlinear threshold electric field (∼8 kV/cm) as before, but the hold-time of the carrier avalanche multiplication is reduced to 30 ns. This enhances the lifetime of the PCSS to ten pulses, as opposed to the single pulse lifetime observed in the previous case.

B. Transmission Line Energy Storage Mode

Through the previous analysis, this paper indicated that the PCSS lifetime is improved by decreasing capacitance to control the hold-time of carrier avalanche multiplication under the

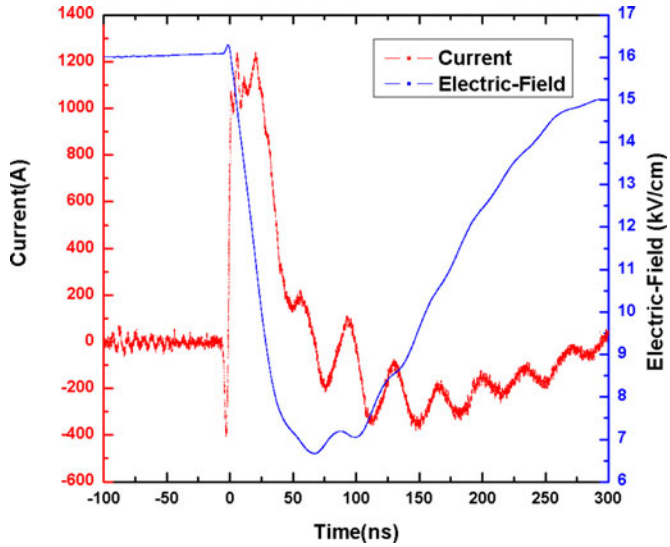

Fig. 14. Current and the electric field characteristic curves of a 3-mm-gap GaAs PCSS.

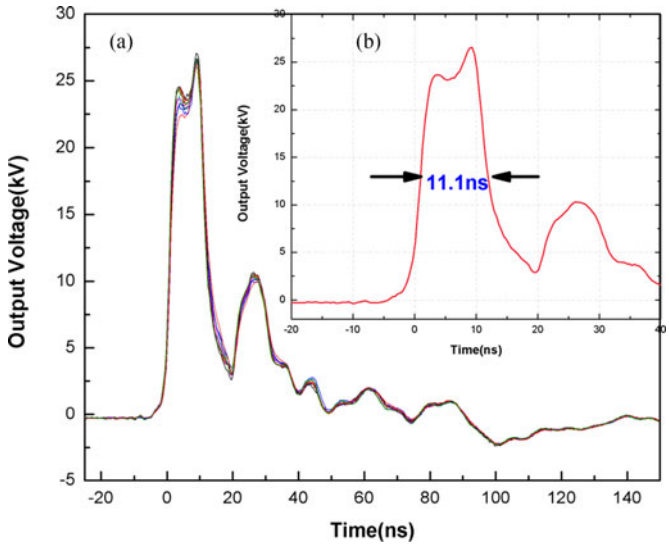

Fig. 15. Output voltage waveform across the load for a 5-mm-gap GaAs PCSS. (a) Ten superimposed waveforms. (b) Single waveform.

capacitor energy storage case. But it is difficult to precisely control the hold-time of carrier avalanche multiplication by changing capacitance. In the case of the transmission line storage, the hold-time of carrier avalanche multiplication can be precisely controlled by the length of transmission line. In order to gain further insight into how to improve the lifetime of a PCSS, a transmission line energy storage test to control the hold-time of the carrier avalanche multiplication was used. In this test, we can control the output pulse width by changing the characteristics of the transmission line.

The dominant mode of electromagnetic wave transmission in the transmission line is the TEM mode. Based on transmission line theory, the characteristic impedance for the TEM mode can be expressed as follows:

$$Z_0 = \sqrt{L_0/C_0} \tag{2}$$

where L_0 and C_0 are the inductance and capacitance per unit length of the transmission line, respectively. The L_0 and C_0 parameters can be expressed by

$$L_0 = \mu_0 \mu_r d/w \tag{3}$$

$$C_0 = \varepsilon_0 \varepsilon_r w/d. \tag{4}$$

Here, w (4 mm) is the width of the silver electrode, d (4 mm) is the thickness of transmission line, $\mu_0 (4\pi \times 10^{-7}$ H/m) and $\mu_r = 1$ are the permeability of vacuum and the relative permeability of the dielectric, respectively, and $\varepsilon_0 (8.85 \times 10^{-12}$ F/m) and ε_r are the permittivity of vacuum and the relative permittivity of the dielectric, respectively. By combining (3) and (4) with (2), the characteristic impedance of the transmission line can be expressed as follows:

$$Z_0 = 377 \frac{d}{w\sqrt{\varepsilon_r}}. \tag{5}$$

The calculated value of the characteristic impedance is 49 Ω. When the laser triggers the GaAs PCSS, the BL has already been charged by the high-voltage pulse. Closing the switch causes the system to output a high-voltage pulse of a certain width onto the load. Based on analysis of the pulse formation process in the BL, the output voltage on the load can be expressed as follows:

$$U_o = \frac{2R_L Z_0}{(Z_0 + R_{\mathrm{PCSS}})(R_L + 2Z_0)} U_i. \tag{6}$$

Here, R_L and R_{PCSS} are the load resistance and the PCSS resistance, respectively, and U_i is input voltage on the PCSS. Equation (6) can be rearranged to obtain R_{PCSS} as follows:

$$R_{\mathrm{PCSS}} = \frac{2R_L Z_0}{(R_L + 2Z_0)} \frac{U_i}{U_o} - Z_0. \tag{7}$$

According to Ohm's law, the current in the PCSS can be expressed as follows:

$$I = \frac{U_i}{(Z_0 + R_{\mathrm{PCSS}})} = \frac{(R_L + 2Z_0)}{2R_L Z_0} U_o. \tag{8}$$

The PCSS resistance and conduction current can be easily calculated from (7) and (8) by measuring the input and output voltages.

In this test circuit, the GaAs PCSS gap is 5 mm and the input voltage of the PCSS is 21 kV. Fig. 15(a) shows ten superimposed waveforms of the output voltage across the load. Fig. 15(b) shows a single pulse, and it can be seen that the circuit outputs a 24 kV pulse with an 11.1 ns duration across the load. Based on BL pulse forming theory, the pulse width of the output voltage (t_{FW}) can be expressed as follows:

$$t_{\mathrm{FW}} = \frac{2l\sqrt{\varepsilon_r}}{c} \tag{9}$$

where l is the length of the transmission line and c is the speed of light. Equation (9) shows that the pulse width of the output voltage depends mainly on the length of the transmission line. When the Nd:YAG laser triggered the PCSS, the current rapidly increased to 404 A. During this time, the PCSS operates in the

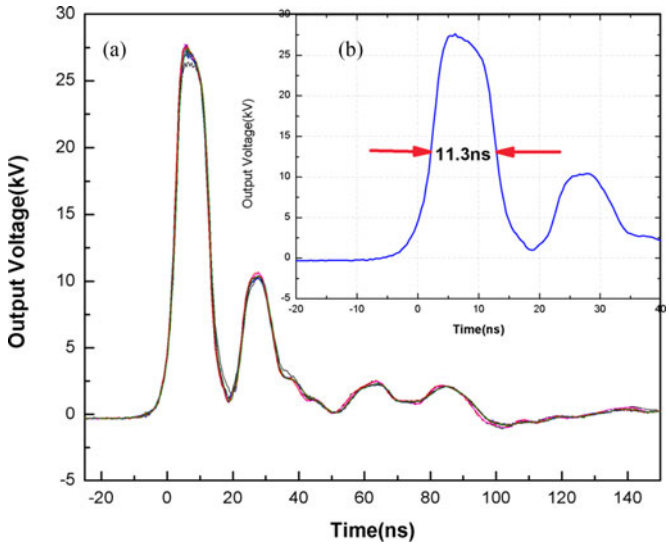

Fig. 16. Output voltage waveform across the load for an 8-mm-gap GaAs PCSS. (a) Ten superimposed waveforms. (b) Single waveform.

TABLE II
SUMMARY OF THE TRANSMISSION LINE TEST PARAMETERS AND RESULTS

The gap of PCSS	5 mm	8 mm
INPUT voltage	21 kV	22 kV
BIAS electric field	42 kV/cm	27.5 kV/cm
CURRENT IN THE PCSS	404 A	438 A
Avalanche time	11.1 ns	11.3 ns
Lifetime	2203 pulses	4635 pulses

nonlinear mode, and the carrier avalanche multiplication phase lasted around 11 ns before the PCSS exited the nonlinear mode. The experimental results showed that the 5-mm-gap GaAs PCSS triggered by the Nd:YAG laser could withstand 2203 pulses before failing.

To improve the lifetime of the PCSS, the gap of the device was increased to 8 mm to reduce the damage caused by the avalanche multiplication. In this test circuit, the input voltage of the PCSS is 22 kV. Fig. 16(a) shows ten superimposed waveforms of the output voltage across the load. Fig. 16(b) shows a single pulse, and it can be seen that the circuit outputs a 26 kV pulse with 11.3 ns duration across the load. When the Nd:YAG laser triggered the PCSS, the current rapidly increased to 438 A. During this time, the PCSS operates in the nonlinear mode, and the carrier avalanche multiplication phase lasted around 11 ns as with the previous test. The experimental results showed that the 8-mm-gap GaAs PCSS triggered by the Nd:YAG laser could withstand 4635 pulses before failing.

The lifetime and other parameters for these two tests are summarized in Table II. This table shows that the bias electric field changed from 42 to 27.5 kV/cm as the gap of the PCSS was increased from 5 to 8 mm. This decrease in the bias electric field increased the lifetime of the PCSS from 2203 pulses to 4635 pulses, which is an increase of more than twofold. When the duration of the carrier avalanche multiplication phase is fixed,

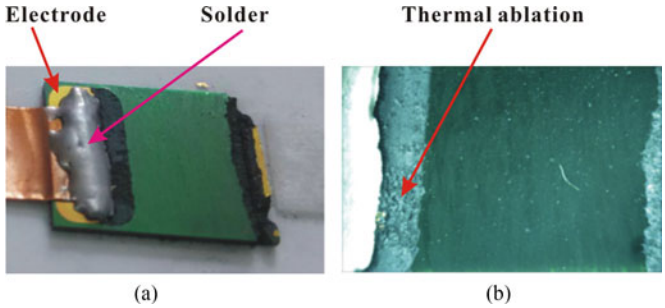

Fig. 17. (a) Image showing the damage to the 5-mm-gap GaAs. (b) Microscopic image of thermal ablation near the electrodes.

the degree of damage is dominated by the degree of avalanche multiplication.

After impact ionization occurs, the carrier avalanche multiplication progress can be expressed as follows:

$$n(t_a) = n_0 \exp(\alpha v_e t_a) \tag{10}$$

where n_0 is the number of photoexcited carriers, v_e is the speed of the carriers, t_a is the avalanche duration, and α is the ionization coefficient which is given by

$$\alpha = A \exp(-B/E_{\mathrm{PCSS}}). \tag{11}$$

Here, *A* and *B* are constants which are determined primarily by the characteristics of the PCSS. It is also observed that the ionization coefficient increases with the bias electric field of the PCSS. According to the previous analysis, decreasing the bias electric field leads to an improvement in device lifetime.

C. Damage Analysis

The 5-mm-gap GaAs PCSS used in the transmission line energy storage test was examined under the microscope to analyze the damage after it was operated in the nonlinear mode for 2203 pulses. The device images are shown in Fig. 17, and it is clear that the regions around the electrodes exhibit more damage than other regions. During the experiment, the electrodes began to exhibit local ablation after 300 pulses, after which erosion started to spread across the entire electrode. At same time, flashover started to appear near the two electrodes of the PCSS. Once the electrode erosion reached the solder, the PCSS failed after 100 additional pulses.

The most important causes of damage to the GaAs PCSS are thermal effects, which are observed to induce electrode erosion during the experiment. The thermal breakdown process of one shot can be expressed as follows:

$$C_V \cdot \frac{dT}{dt} = \sigma E^2 \tag{12}$$

where C_V is the specific heat of the GaAs PCSS, σ is the conductivity of GaAs, and *E* is the bias electric field. The term σE^2 on the right-hand side of the equation expresses the joule heating generated from the current flow. In the nonlinear mode of operation, current filaments were observed between the two electrodes, and these are the main cause of thermal damage to the PCSS. The diffusion terms can be ignored due to the

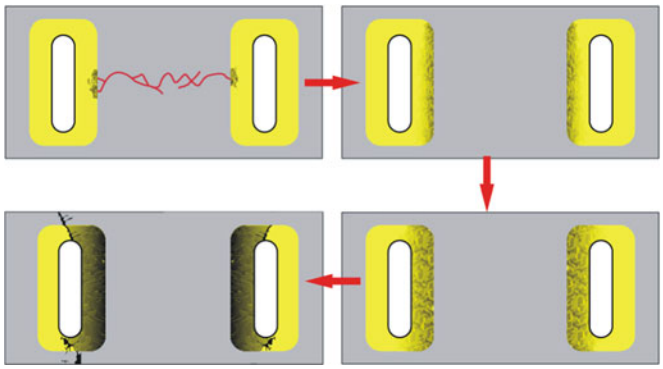

Fig. 18. Gradual development process of electrode erosion and PCSS failure.

transient and adiabatic nature of process of the single shot. So, the temperature increase of a current filament channel can be expressed as follows:

$$\Delta T = \left[\left(\frac{U_i}{Z_0 + R_{\mathrm{PCSS}}}\right)^2 R_{\mathrm{PCSS}} \Delta t\right] / \left(\rho \pi {r_c}^2 l C_v\right) \tag{13}$$

where r_c and l are the radius and length of the current filament channel, respectively. In this experiment, the ON-state resistance (R_{PCSS}) was 2.87 Ω, the ON-time (Δt) was 11.1 ns, and the repetition frequency (f) was 10 Hz. The GaAs density (ρ) is 5.371 g·cm^{-3} and the specific heat of the GaAs PCSS is 0.36 J·g^{-1}·K^{-1}. The calculated value of ΔT is then 57.34 K. Considering this analysis, the temperature of the GaAs PCSS surface increases with the number of trigger pulses. Under the multishots condition, it is necessary to account for diffusion terms. The temperature increase of the GaAs PCSS surface is proportional to the repetition frequency.

Based on the previous analysis, thermal damage to the structure develops gradually. A percolation theory is used to explain the failure, and this process is shown in Fig. 18. As mentioned earlier, the temperature of the GaAs PCSS surface increases with the number of trigger pulses. The melting temperature of the photoconductive electrode and SI-GaAs crystals is ∼350 and 1238 °C, respectively, which means that the damage to the GaAs PCSS begins at the electrodes.

First, because the current path through the device in the nonlinear mode of operation is through filaments, the thermal damage is generated in the contact zone between the electrode and a current filament. The current filament path is usually random, so these thermal breakdowns cause erosion at the electrode borders which increases with the number of trigger pulses. Second, erosion of the electrode border results in a degradation of the ohmic contact performance, which causes the corrosion rate to accelerate. Finally, when the erosion of the electrode progresses to the solder, flashover occurs between the solder and the GaAs wafer, which is followed by heat stress damage. On one hand, the stresses cause local microcosmic fractures near the electrodes. When these local microcosmic fractures reach a critical density level, macrofractures occur, and disintegration of the high-power PCSS can even occur. On the other hand, the electrode erosion is so slow that the switch remains effective until the alloy of the electrodes is exhausted. In summary, electrode erosion and stress damage are the two leading factors that induce the failure of a high-power PCSS.

IV. Conclusion

This paper has presented the results of two typical lifetime tests of high-power GaAs PCSSs under different energy storage modes. Under the capacitive energy storage mode, the lifetimes of a 2-mm-gap GaAs PCSS with a 470 nF capacitor and an output current of 1.3 kA and a 3-mm-gap GaAs PCSS with a 30 nF capacitor and an output current of 1.21 kA were one and ten pulses, respectively. Under the transmission line energy storage mode, the lifetimes of a 5-mm-gap and an 8-mm-gap GaAs PCSS with output currents of 404 A and 438 kA were 2203 and 4635 pulses, respectively. Additionally, the impact of various factors on the device lifetime was discussed. Under the capacitive energy storage mode, the hold-time of the carrier avalanche multiplication depends on the capacitance size. The capacitance was reduced from 470 to 30 nF to reduce the hold-time of the carrier avalanche multiplication and improve the lifetime of the PCSS. Under the transmission line energy storage mode, the hold-time of the carrier avalanche multiplication was precisely controlled by the transmission line length. The transmission line energy storage mode showed that the PCSS lifetime improved by changing bias electric field to control the avalanche degree. It was also seen that decreasing the bias electric field changed the degree of carrier avalanche multiplication, which improved the lifetime of the PCSS.

Finally, we have analyzed the failure mechanisms seen in these devices. A percolation theory was used to explain the failures. The current filament caused erosion of the electrode border, which increased with the number of trigger pulses. When the erosion of the electrode progressed to the solder, flashover occurred between the solder and the GaAs wafer, and this was followed by heat stress damage. In summary, electrode erosion and stress damage are the two leading factors that induce the failure of a high-power PCSS.

References

[1] F. J. Zutavern *et al.*, "Photoconductive semiconductor switch experiments for pulsed power applications," *IEEE Trans. Electron Devices*, vol. 37, no. 12, pp. 2472–2477, Dec. 1990.

[2] S. Ajram and G. Salmer, "Ultrahigh frequency DC-to-DC converters using GaAs power switches," *IEEE Trans. Power Electron.*, vol. 16, no. 5, pp. 594–601, Sep. 2001.

[3] V. Pala, H. Peng, P. Wright, M. Mostafa Hella, and T. Paul Chow, "Integrated high-frequency power converters based on GaAs pHEMT: Technology characterization and design examples," *IEEE Trans. Power Electron.*, vol. 27, no. 5, pp. 2644–2656, May 2012.

[4] J. S. H. Schoenberg, J. W. Burger, J. S. Tyo, M. D. Abdalla, M. C. Skipper, and W. R. Buchwald, "Ultra-wideband source using gallium arsenide photoconductive semiconductor switches," *IEEE Trans. Plasma Sci.*, vol. 25, no. 2, pp. 327–334, Apr. 1997.

[5] G. M. Loubriel, M. W. O'Malley, and F. J. Zutavern, "Toward pulsed power uses for photoconductive semiconductor switches: Closing switches," in *Proc. 6th Pulsed Power Conf.*, Arlington, VA, USA, 1987, pp. 145–148.

[6] F. J. Zutavern, G. M. Loubriel, M. W. O'Malley, W. D. Helgeson, and D. L. McLaughlin, "High gain photoconductive semiconductor switching," in *Proc. IEEE Pulsed Power Conf.*, 1991, pp. 23–28.

[7] W. Shi, C. Ma, L. Hou, G. Xie, L. Tian, and S. Wu, "Velocity of current filament at the high gain mode of GaAs power photoconductive switches," *Physica B*, vol. 406, no. 19, pp. 3741–3744, 2011.

[8] A. Mar *et al.*, "Fireset applications of improved longevity optically activated GaAs photoconductive semiconductor switches," in *Proc. IEEE Pulsed Power Plasma Sci. Conf.*, 2001, pp. 166–169.
[9] A. Mar *et al.*, "Multi-filament triggering of PCSS for high current utilizing VCSEL triggers," in *Proc. IEEE Int. Pulsed Power Plasma Conf.*, 2007, pp. 1000–1003.
[10] J. L. Hudgins, G. S. Simin, E. Santi, and M. A. Khan, "An assessment of wide bandgap semiconductors for power devices," *IEEE Trans. Power Electron.*, vol. 18 no. 3, pp. 2644–2656, May 2003.
[11] F. J. Zutavern *et al.*, "DC-charged GaAs PCSSs for trigger generators and other high-voltage applications," *IEEE Trans. Plasma Sci.*, vol. 38, no. 10, pp. 2708–2715, Oct. 2010.
[12] C. Ma, W. Shi, M. Li, H. Gui, N. Hao, and P. Xue, "Impact of current filaments on the material and output characteristics of GaAs photoconductive switches," *IEEE Trans. Electron Devices*, vol. 61, no. 7, pp. 2432–2436, May 2014.
[13] W. Shi, C. Ma, and M. Li, "Research on the failure mechanism of high-power GaAs PCSS," *IEEE Trans. Power Electron.*, vol. 30, no. 5, pp. 2427–2434, May 2015.
[14] W. Shi, X. Wang, and L. Hou, "Lower bound of electrical field for maintaining a GaAs photoconductive semiconductor switch in high-gain operating mode," *IEEE Trans. Electron Devices*, vol. 60, no. 4, pp. 1361–1364, Apr. 2013.
[15] W. Shi *et al.*, "Investigation of electric field threshold of GaAs photoconductive semiconductor switch triggered by 1.6J laser diode," *Appl. Phys. Lett.*, vol. 104, no. 4, pp. 042108–042111, Jan. 2014.

Authors' photographs and biographies not available at the time of publication.